NASA CR-775

IONIZATION PROBABILITY OF IRON PARTICLES AT METEORIC VELOCITIES

By J. C. Slattery and J. F. Friichtenicht

Prepared under Contract No. NASw-1336 by
TRW SYSTEMS
Redondo Beach, Calif.

for

NATIONAL AERONAUTICS AND SPACE ADMINISTRATION

For sale by the Clearinghouse for Federal Scientific and Technical Information
Springfield, Virginia 22151

IONIZATION PROBABILITY OF IRON PARTICLES AT METEORIC VELOCITIES*

by J. C. Slattery and J. F. Friichtenicht
TRW Systems, Redondo Beach, California

ABSTRACT

The number of ion pairs produced by the total ablation of iron particles in air and argon was measured as a function of particle velocity. Micron size iron particles of known mass and velocity were injected into a gas target chamber and the resultant ionization collected with a parallel plate ionization chamber. Initial velocities of the particles ranged from 20 km/sec to 45 km/sec. The ionization probability β, for an iron particle in argon was found to be $\beta = 2.75 \times 10^{-20} v^{4.13}$, where v is the particle velocity in meters/sec. The ionization probability of an iron particle in air was found to be $\beta = 2.60 \times 10^{-15} v^{3.12}$, with v in meters/sec.

*This work supported by the NASA under Contract NASW-1336.

Preceding page blank

IONIZATION PROBABILITY OF IRON PARTICLES AT METEORIC VELOCITIES*

by J. C. Slattery and J. F. Friichtenicht
TRW Systems, Redondo Beach, California

1. INTRODUCTION

One of the principal objectives of ground-based meteor observations is to obtain the mass and density of the meteoroid under study. The two most commonly employed techniques are photographic analysis of the luminous trail and radar probing of the ionized wake. Contemporary meteor theory (see Whipple and Hawkins[1] or McKinley[2] for a summary) provides a framework for relating the measured quantities to the quantities of primary interest. However, the values of some of the parameters utilized in meteor theory are not accurately known. Presently accepted values are based on phenomenological observation of natural meteors, and the possible errors are admitted to be large.

This paper gives the results of experiments in which meteor ionizing efficiency has been determined directly by laboratory simulation of meteor entry. Because of the straightforward techniques employed, it is believed that this experiment yields an accurate value for meteor ionizing efficiency. The results are consistently higher than those obtained by analytical means. More specifically, the measured ionizing probability is significantly greater than that predicted by Öpik[3] on the basis of a theoretical treatment of atomic interactions and almost a factor of ten higher than that obtained by Verniani and Hawkins[4] from observation of natural meteors.

The ionizing efficiency is the fraction of the meteoroid energy which is used to make ions. It is usually defined in terms of the ionizing probability β. β is the probability that a single ablated meteor atom will produce an ion pair as it is thermalized by collisions with the gas

*This work supported by the NASA under Contract NASW-1336.

molecules. Of course, β is velocity dependent. The ionizing efficiency is related to β by

$$\tau_q = \frac{2\phi}{\mu v^2} \beta \tag{1}$$

where ϕ is the ionization energy of the atom being ionized and μ and v are the mass and velocity of the ablated atom.

2. LABORATORY METEOR SIMULATION

For adequate simulation of meteoric phenomena in the laboratory, certain conditions must be satisfied. One of the most stringent requirements is imposed by aerodynamic considerations. Most radio and photographic meteors are observable at altitudes where free molecular flow conditions prevail. The free molecular regime is specified by the condition that the molecular mean free path be much larger than typical body dimensions, i.e., $\lambda/D >> 1$, where λ is the molecular mean free path and D the particle diameter. Thus, the larger the body, the lower the absolute gas pressure must be. An obvious consequence of lowered gas pressure is increased interaction distance; even a casual evaluation indicates that reasonable interaction distances can be achieved only by the use of small particles.

The particle accelerator described by Friichtenicht[5] provides high-velocity particles that meet the required conditions. In this device, small conducting particles are charged by contact with a charging electrode maintained at a high positive potential with respect to its surroundings. The charged particles are injected into the accelerating field of a commercial two-million-volt Van de Graaff accelerator.* Slattery et al.[6] have presented data on drag and heat transfer coefficients obtained with this accelerator and described the application of the accelerator to meteor simulation experiments.

*Manufactured by High Voltage Engineering Corporation

Provided the general mechanism used to describe ion production is correct, there appears to be no difficulty in applying the experimental results to natural meteors, even though the absolute sizes of the particles are significantly different. It appears that vaporization is the primary method of mass loss for the experimental particles. Atoms evaporated from the particles travel through the gas at essentially particle velocity and suffer collisions with the air molecules. Before an evaporated atom loses all of its kinetic energy by collisions there is some probability β that either an iron or an air molecule will be ionized. This is exactly the mechanism employed to describe meteor ionization.

The absolute gas pressure used in these experiments is much higher than the atmospheric pressure in the region where meteors appear. However, the particles are so small that $\lambda/D > 5 \times 10^3$ for the worst case, and the conditions for free molecular flow are thus certainly satisfied.

A particle of mass m and velocity v entering an atmosphere of density ρ is decelerated at the rate

$$\frac{dv}{dt} = - \frac{\Gamma A \rho v^2}{m} \tag{2}$$

where Γ is the drag coefficient and A is the projected area of the meteor. The rate of mass loss is given by

$$\zeta \frac{dm}{dt} = - \frac{\lambda}{2} A \rho v^3 \tag{3}$$

where ζ is the heat of ablation and λ is the (dimensionless) heat transfer coefficient.

The change in particle mass with velocity may be obtained by dividing Eq. (3) by Eq. (2) and integrating from an initial velocity v_o to a velocity v. The result is

$$m = m_o \, e^{- \frac{\sigma}{2} (v_o^2 - v^2)} \tag{4}$$

where $\sigma = \lambda/2\Gamma\zeta$.

The implications of Eq. (4) are pointed out by Table I, where the change in velocity as a function of initial velocity is given for 99% mass ablation, i.e., $m/m_o = 0.01$. The calculations are based on $\Gamma = 1$, $\Lambda = 1$ (from Ref. 6), and $\zeta = 7.2 \times 10^{10}$ ergs/gm (heat of vaporization of iron).

TABLE I. Deceleration for 99% Mass Ablation ($m/m_o = 0.01$)

Initial Velocity (km/sec)	Final Velocity (km/sec)	Fractional Velocity Change
40.0	38.4	.04
30.0	27.7	.09
25.0	22.2	.11
20.0	16.4	.18
15.0	9.7	.35

It can be seen that a particle with a high initial velocity is essentially completely vaporized while suffering negligible deceleration. The actual magnitude of the velocity change is dependent upon σ; however, relatively large uncertainties in σ can be tolerated without significantly affecting the basic assumption. If constant velocity is assumed, the total number of ion pairs produced by the particle is related directly to the number of atoms in the particle through the ionization probability β.

$$N_{ions} = \beta N_{atoms} \tag{5}$$

Thus measurement of the number of ions produced as a function of initial particle velocity gives directly β as a function of velocity if the initial particle mass is known.

3. EXPERIMENTAL TECHNIQUES AND APPARATUS

A diagram of the experimental configuration is shown in Fig. 1. Charged particles from the accelerator pass first through two particle detectors used to measure the particle velocity and then through a third detector from which the charge on the particle is determined. The particles enter the gas target region after passing through the apertures of a differential pumping system. Ions produced in the chamber are collected on one plate of a parallel-plate ionization chamber. Photomultiplier tubes (not shown in the figure) spaced along the ionization chamber view the luminous trail and serve to indicate the position of the particle while ionization is occurring. The pressure within the gas chamber is adjusted by a variable leak and is monitored by a Pirani gauge. The function and operation of each of these items is discussed below.

3.1 INITIAL PARTICLE PARAMETER MEASUREMENT

The magnitude of the charge on a particle entering the test setup is determined by measuring the amplitude of a voltage signal induced on a cylindrical drift tube of known capacitance through which the particle passes. Its velocity is determined by measuring the transit time through a single detector or the travel time between detectors set a known distance apart. Given charge q and velocity v, the particle mass is computed from the conservation of energy equation: $(1/2)\ mv^2 = qV$, where V is the total accelerating voltage.

Only a small fraction of the particles from the accelerator are compatible with a given set of experimental conditions. For a given gas pressure, there are limits on particle velocity and mass which will result in total vaporization of the particle while it is within the confines of the ionization chamber. The principal function of the velocity discriminator

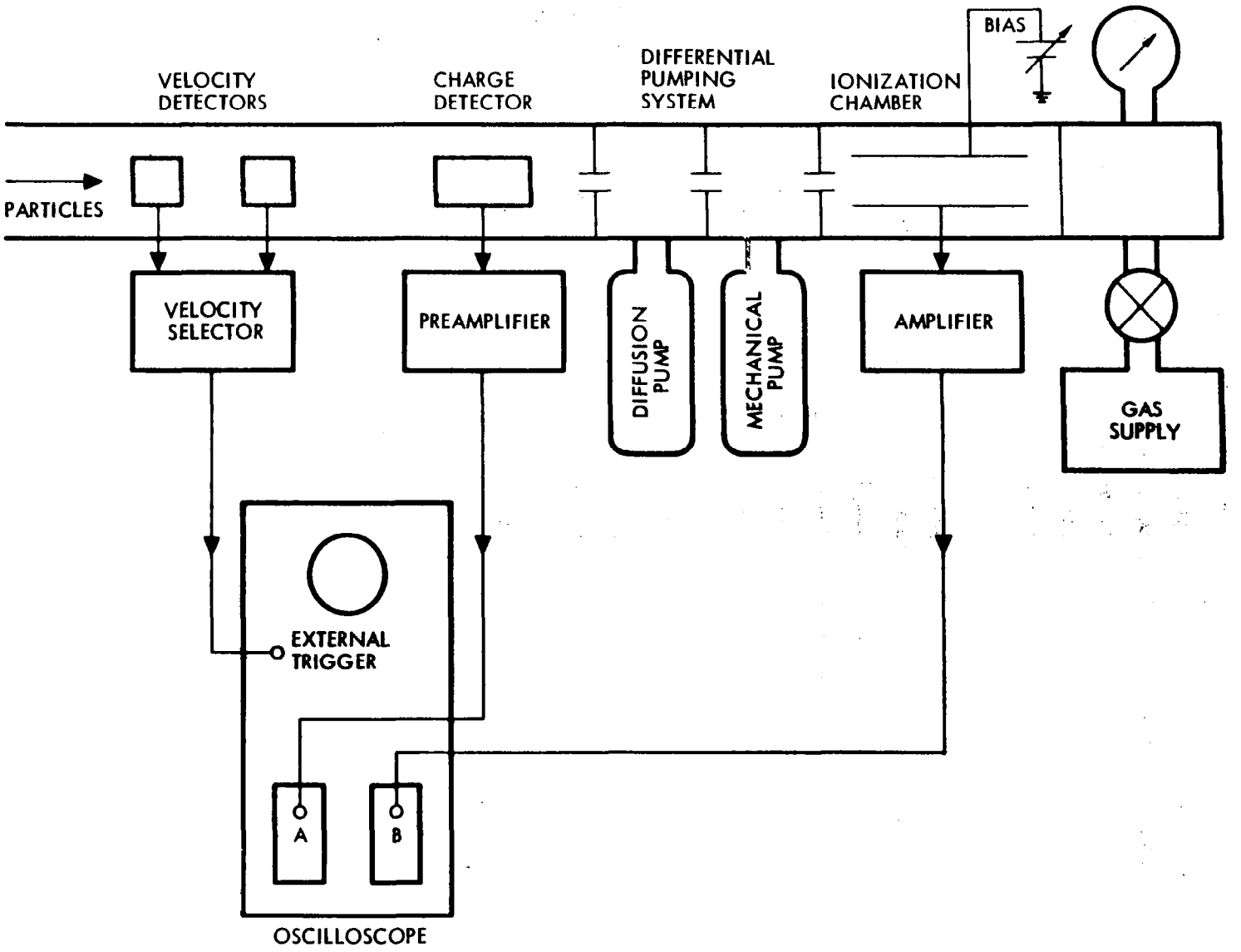

Figure 1. Block Diagram of Experimental Configuration

is the selection of events to be displayed on the recording oscilloscopes. Signals from the two velocity detectors are fed to an electronic logic circuit, and if the particle transit time between the detectors lies within a preset interval, a trigger pulse is generated. The trigger pulse, which is coincident with the leading edge of the signal from the second velocity detector, is used to start the sweep of a dual-beam oscilloscope (Tektronix Model 555). Since the velocity of particles from the accelerator depends upon their mass,[5] the selection of a velocity range specifies the mass range also.

The velocity of each particle is determined more precisely by measuring its transit time between the second velocity detector and the charge detector. This is accomplished by displaying the charge detector signal on the oscilloscope trace triggered by the output pulse from the velocity discriminator. The transit time between the detectors, which are separated by 77.5 cm, is measured from the beginning of the trace to the leading edge of the charge detector pulse. The uncertainty in the velocity measurement is estimated to be less than $\pm 2\%$.

Since the q/m ratio of particles from the accelerator is inversely proportional to particle size, one must use extremely small particles (typically 0.1 micron in diameter for the present work) to obtain sufficiently high velocities. Particles in this size range carry a charge of between 2×10^{-16} and 2×10^{-15} coulombs. The charge detector utilizes a high input impedance preamplifier[7] connected in a bootstrapped configuration. The amplitude of the output signal V_c is related to the particle charge by $q = V_c C/G$, where C is the detector capacitance and G is the preamplifier gain. The quantity C/G is not amenable to direct measurement in the bootstrapped configuration; it was determined by direct comparison of the signal with that of a calibrated charge detector that utilized a conventional cathode-follower input stage. The capacitance of the comparison detector (including the input capacitance of the amplifier) was measured with a precision capacitance bridge, and the gain was determined by amplifying a signal of precisely known amplitude. The two detector-preamplifier combinations were compared by measuring the amplitude

of the respective output signals produced by a common particle from the accelerator. Since the comparison detector is less sensitive, the range of particle charges used for calibration was from 10^{-14} to 10^{-13} coulombs. The estimated uncertainty in the calibration of C/G for the charge detector is $\pm$10%.

Another factor that influenced the precision of the charge measurement was the signal-to-noise ratio, which was about 3 for the worst case (highest-velocity particles) and greater than 10 for the low-velocity particles. The difficulty in reading the charge precisely contributed to the spread in the final data. The reading error was estimated at less than $\pm$20% for high-velocity particles and less than $\pm$5% for particles at low velocities.

3.2 IONIZATION MEASUREMENT

The ionization chamber consisted of a pair of gold-plated parallel plates 30.6 cm long and 2.5 cm wide, separated by 0.64 cm. The particles were injected along a plane midway between the two plates. One of the plates was connected to a positive bias supply, which was varied from 10 to 50 volts, while the other, which served as the ion collector, was grounded through the input stage of a high input impedance solid state amplifier. The amplifier had an overall voltage gain of about 100 and a pass band from 100 cps to 1 Mc/sec. The RC decay time of the input stage (which included the capacitance to ground of the collector plate) was fixed at about 0.5 sec. Since this period was very long in comparison with the time interval over which ions were collected, the ion current was effectively integrated at the input stage. The total charge collected Q_c was related to the amplitude of the output signal V_o by $Q_c = V_o C_c/G$, where C_c is the capacitance of the collector and G is the voltage gain of the amplifier.

The ionization chamber was calibrated by applying a pulse of known amplitude through a calibrated capacitor C_o to the input of the amplifier and measuring the ratio of output voltage to input voltage. This quantity is equal to $GC/(C + C_o)$, where C is the capacitance of the chamber,

including the amplifier input capacitance, and G is the voltage gain. During operation the calibrating capacitor remained in place, but it was returned to ground, giving an effective collector capacitance $C_c = C + C_o$. The uncertainty in the measured value of C_c/G is estimated to be less than $\pm 5\%$, and random errors due to reading the pulse amplitude are estimated to be less than $\pm 3\%$.

The transition from the main accelerator vacuum system to the low-pressure gas target was accomplished by means of a differential pumping system. The system contained two intermediate pressure chambers, one of which was continually evacuated by an oil diffusion pump while the other was pumped by a mechanical fore-pump. Particles from the accelerator were injected through the channels separating the various chambers. The system was capable of sustaining target pressures up to about 5 Torr, although the maximum pressure required for the present experiment was only about 0.1 Torr. The only particular requirement imposed on the gas pressure was that it be within the range in which a particle would be vaporized while within the space occupied by the ionization chamber plates. Since the absolute gas pressure was not particularly critical, no attempt to measure it precisely was made. Instead, the pressure was simply monitored by a calibrated Pirani gauge. Regulation and adjustments were made by means of a variable leak.

The correct pressure to be used for any given particle velocity and mass range was determined by inspection of the signals obtained from the photomultiplier tubes and the ion collector (see Fig. 1). If the pressure was too high, vaporization and ionization started within the entrance channel and some of the ions were not collected, as evidenced by an abruptly rising ionization signal and no luminous emission towards the downstream end of the chamber. If the pressure was too low, vaporization did not commence early enough and the particle left the chamber with a residual mass. This type of behavior was manifested by significant luminosity at the last photomultiplier tube and a sudden break in the ionization signal, indicating that the particle was still producing ions as it left the chamber. In practice, the pressure was adjusted so that complete

vaporization took place between the positions specified by phototubes 2 through 5. (There were six phototubes altogether.)

The voltage applied to the collector plate of the ionization chamber was dictated by conflicting requirements. At high values of applied voltage and target chamber pressure, electron multiplication might produce a significant effect, whereas at low pressures and small voltages, a small fraction of the most energetic ions could surmount the potential barrier and reach the positive plate. To avoid the complication of adjusting collector voltage as the pressure was changed, data were collected over the entire range of pressures at collection voltages of 10, 20, and 50 volts. A calculation of the magnitudes of the two opposing effects indicated that they might alter the results by about 10% in the extreme cases. No significant differences in the data acquired at different bias voltages were noted, and all the data were combined.

A reproduction of a typical photographic record is shown in Fig. 2. The charge detector signal is displayed on the upper trace, and the output signal from the ionization chamber is displayed on the lower trace. In operation, the lower trace was triggered automatically by the upper beam sweep. A variable delay between the start of the two sweeps was available, and this was usually selected so that the lower sweep started immediately after the particle passed through the charge detector. The start of the lower beam sweep is signalled by the brightening of the upper trace.

A companion photograph (not shown) recorded the output pulses from the phototubes. This record was used primarily as a qualitative aid in adjusting target pressure and particle parameters. All of the oscilloscope photographs were read on a Telereader projector to three-figure accuracy.

4. RESULTS AND DISCUSSION

The value of β was computed for each particle by dividing the number of ions produced by the number of atoms in the iron particle. The results are plotted in Figs. 3 and 4.

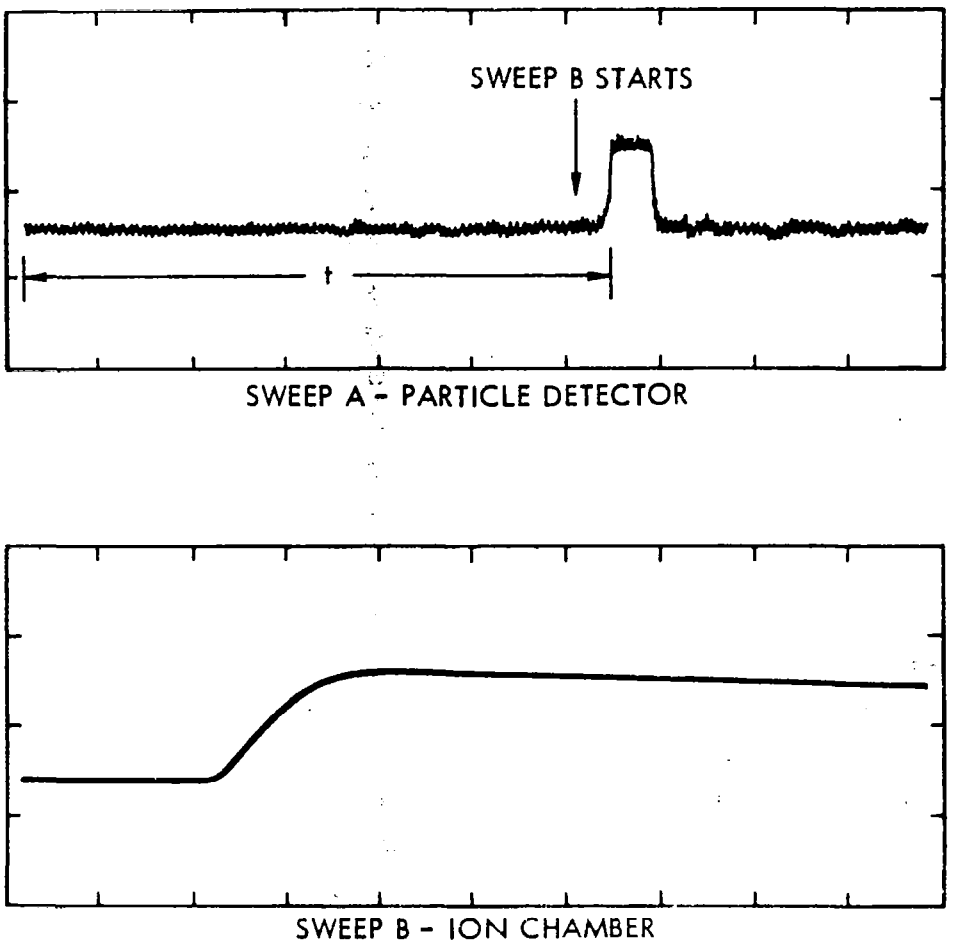

Figure 2. Tracings of oscilloscope pictures obtained for a typical particle. Sweep A is started by the passage of the particle through the second velocity detector and displays the output of the charge detector. The time t is the particle flight time over 77.5 cm and the height of the signal indicates the particle charge. Sweep B is started automatically by Sweep A and displays the output signal from the ion chamber in the gas target. Oscilloscope settings for this particular particle were: Sweep A vertical sensitivity 0.02 volts/cm, horizontal sweep speed 5 μsec/cm, Sweep B vertical sensitivity 2.0 volts/cm, horizontal sweep speed 5 μsec/cm.

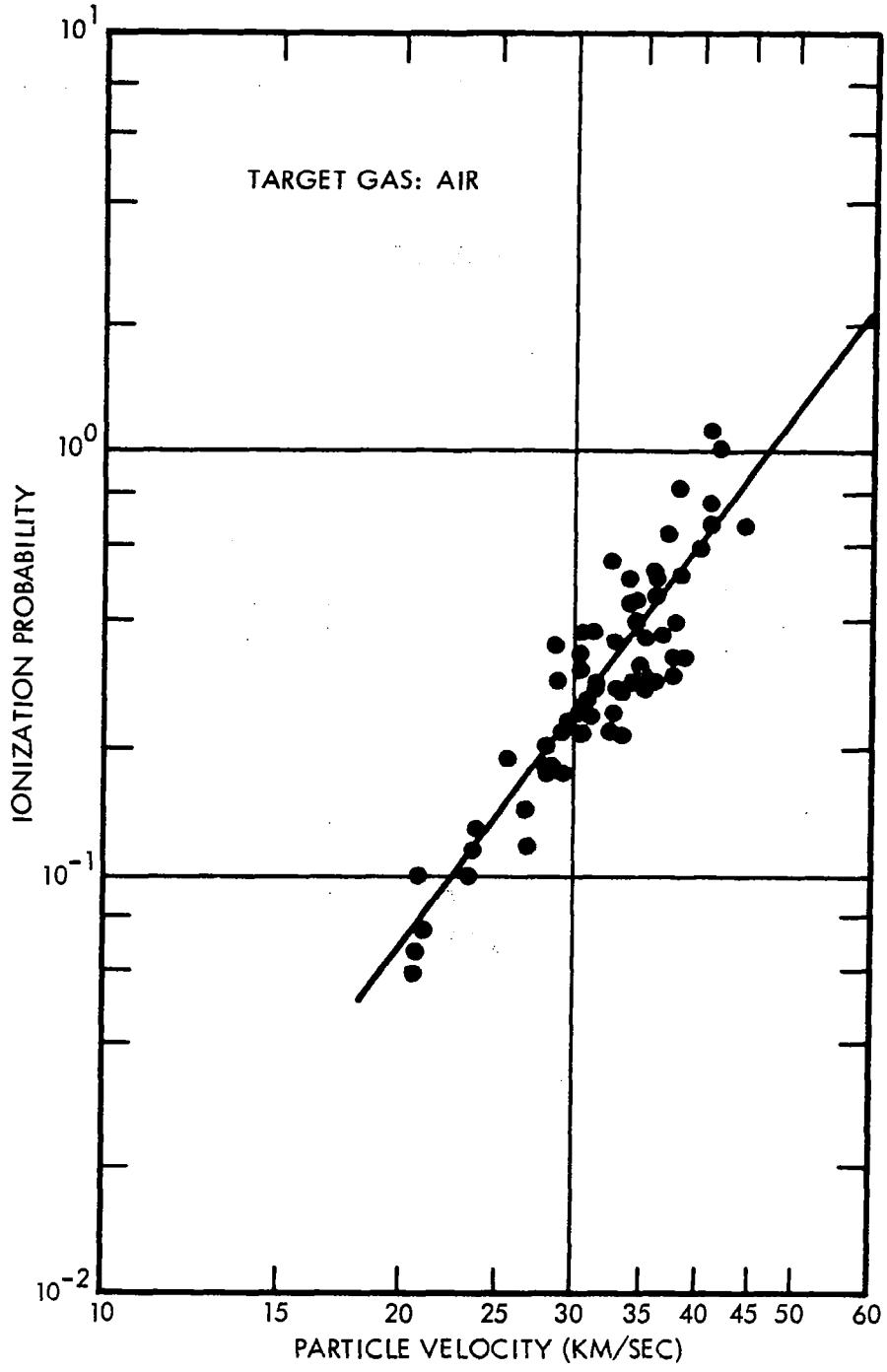

Figure 3. Results of measurements of the ionization probability, β, in air versus the initial velocity of the particle. Each point represents a measurement from one particle. The straight line is a least squares fit to the equation $\log \beta = \log \beta_o + \eta \log v$.

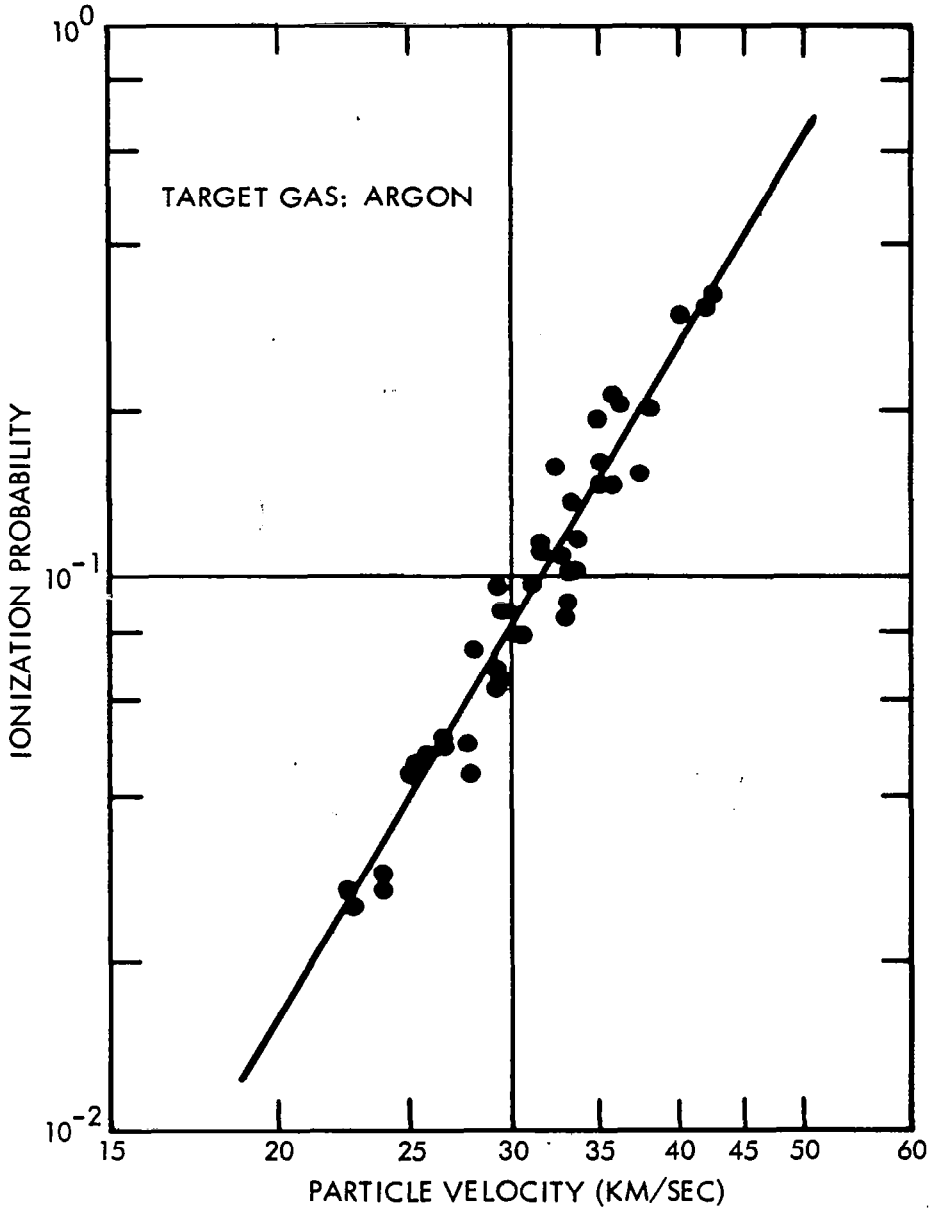

Figure 4. Results of measurements of the ionization probability, β, in argon versus the initial velocity of the particle. Each point represents a measurement from one particle. The straight line is a least squares fit to the equation $\log \beta = \log \beta_o + \eta \log v$.

Figure 3 shows the measured values of β as a function of initial particle velocity with air as the target gas. A similar plot for an argon gas target is shown in Fig. 4. The straight line in each figure is derived from a least-squares fit to the equation

$$\log \beta = \log \beta_o + \eta \log v \quad . \tag{6}$$

Use of this equation assumes that the velocity dependence of β is of the form $\beta = \beta_o v^{\eta}$, which may not be the case.

The results of the least-squares fits to the logarithmic equation, when v is given in m/sec, are

$$\text{Target gas, air:} \quad \log \beta = -(14.585 \pm .118) + (3.12 \pm .19) \log v \tag{7}$$

$$\text{Target gas, argon:} \quad \log \beta = -(19.561 \pm .084) + (4.13 \pm .20) \log v \tag{8}$$

with the standard deviations of the coefficients indicated.

The standard deviations of the coefficients provide a measure of the precision of the results. The accuracy of β_o depends upon the various possible systematic errors discussed in the previous section, which are estimated to total less than $\pm 18\%$. This figure applies to the measurements made with both air and argon targets. The accuracy to which the coefficient η is known is independent of the instrumental errors, since it involves only ratios of β's at different velocities. Thus, the uncertainty in η is indicated by the measured standard deviation. However the values of η depend heavily on a few points on the extremes of the curves, and the standard deviations may give an illusory impression of more accuracy than is really there.

There is no a priori reason for expecting the ionizing efficiency in air to be equal to that in argon. However, one might expect the velocity dependence to be the same, but it appears to differ. Although there is no direct experimental evidence to support such a hypothesis, a possible explanation might be the differences in interaction between

diatomic and monatomic molecules.

It is of interest to compare the results of the present measurements with those obtained by other workers. The most recent calculation of β is probably that of Verniani and Hawkins.[4] They have taken the results of simultaneous photographic and radio observations of meteors and deduced a value for the ratio of luminous efficiency to ionizing efficiency as a function of meteor velocity. From this ratio they then calculate β and its dependence on velocity, using an expression for the luminous efficiency as derived by Verniani.[8] Their resultant expression for the ionizing efficiency of cometary material is

$$\beta = 1 \times 10^{-20} v^4 \qquad (9)$$

where the velocity is in m/sec. The uncertainty in the exponent is estimated by the authors as ± 0.5.

Comparison of the results of Verniani and Hawkins to the present work is complicated by the differences between cometary material and iron. A theoretical calculation by Lazarus and Hawkins[9] on ionizing probability indicates that the relative ionizing efficiencies of different elements vary as the ratios $n\mu/E^6$, where n is the number of valence electrons of the atom, μ is the reduced mass of the atom, and E is the ionization energy. They conclude that the conversion factor between iron and cometary material is

$$\beta_{Fe} = 2.9\ \beta_{cometary} \quad . \qquad (10)$$

For the sake of showing a comparison, we arbitrarily multiply Verniani and Hawkins' result by this factor to obtain

$$\beta_{Fe} = 2.9 \times 10^{-20} v^4 \quad . \qquad (11)$$

A theoretical calculation of the ionizing probability for iron

particles has been made by Öpik,[3] and his results require no correcting to be compared directly to the present results.

The three curves shown in Fig. 5 represent β_{Fe} from the present work, Öpik's value of β_{Fe} and β_{Fe} deduced from the value of $\beta_{cometary}$ obtained by Verniani and Hawkins. It can be seen that the curve representing the present work gives substantially larger values of β_{Fe} than the other two curves. No explanation is offered for this disagreement. However the experimental technique is straightforward and it is difficult to see how the measured values can be in error by a factor of ten.

The form of the velocity dependence suggested by Verniani and Hawkins appears to be compatible with the experimental results, but the value of the exponent is somewhat different. The best fit to the experimental data on the ionizing probability for iron atoms in air is given by the relation

$$\beta_{Fe} = 2.60 \times 10^{-15} v^{3.12} \qquad (12)$$

where the velocity is in units of meters/sec.

There are two considerations that might affect the application of these measurements to meteor physics. First, the time between collisions of atoms is much shorter in the present experiment than in the case of a real meteor, (because of the higher gas density). This leads to the possibility of ionization from an excited state, which is relatively improbable in the case of meteors. This effect would tend to increase the measured value of β. Secondly, the air molecules in this experiment are diatomic, as are atmospheric molecules up to about 100 km altitude, but above 100 km an increasing fraction of the atmosphere is monatomic. The difference in ionizing probabilities for diatomic molecules and monatomic molecules is not known nor can they be deduced from these experiments alone. However, at altitudes around 100 km, the dominant interaction of meteor atoms is with diatomic molecules, to which these experimental results apply directly.

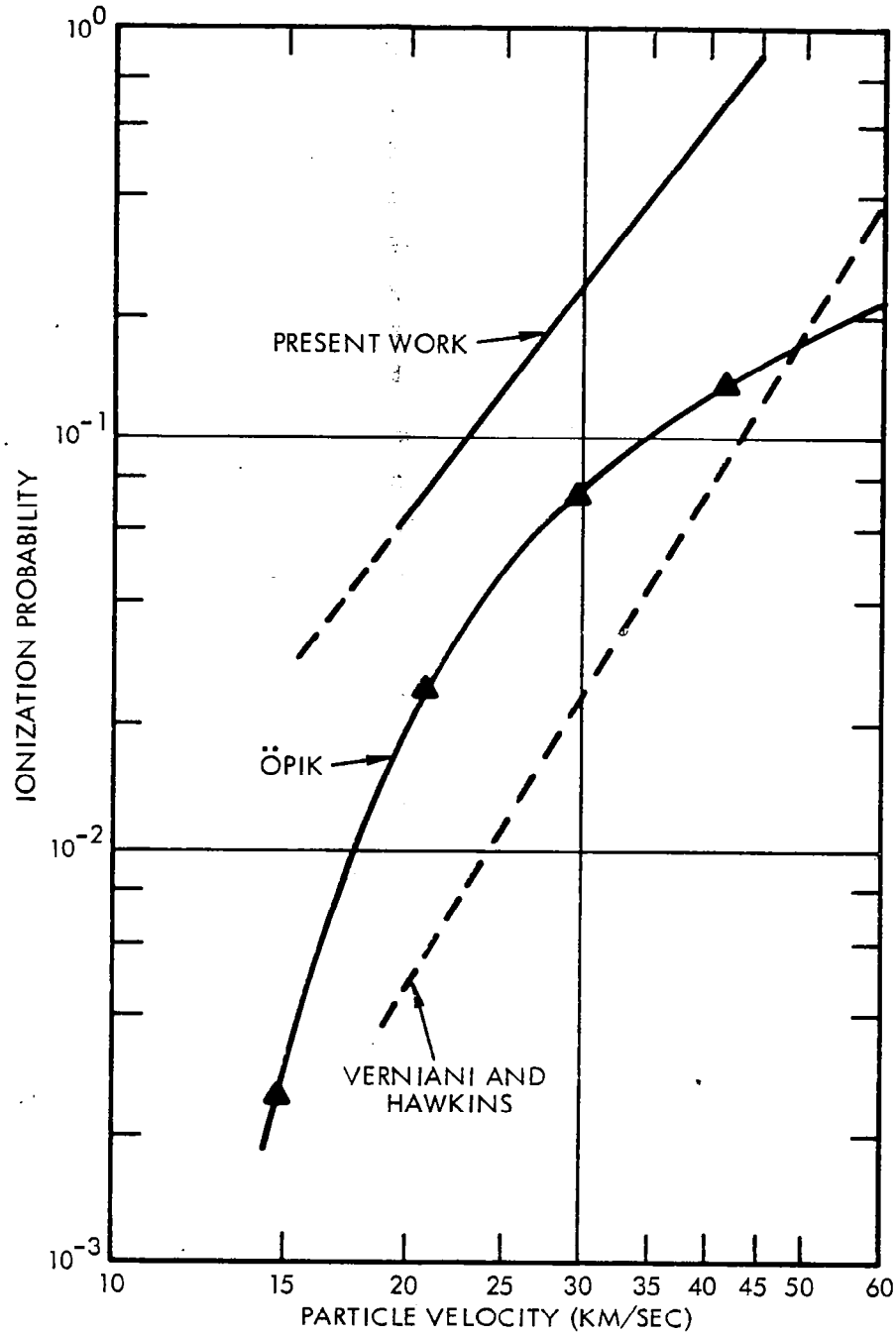

Figure 5. Comparison of the results of the present work to those of Öpik and Verniani and Hawkins. The equation of Verniani and Hawkins has been corrected for the difference between iron and cometary material using the technique of Lazarus and Hawkins.

Experiments are planned to investigate more thoroughly effects of the molecular characteristics of the target gas and of particle material.

REFERENCES

1. F. L. Whipple and G. S. Hawkins, "Meteors," Handbuch der Physik (Springer-Verlag, Berlin, 1959), Vol. III.

2. D. W. R. McKinley, "Meteor Science and Engineering," (McGraw-Hill Book Company, Inc., New York, 1961.)

3. E. J. Öpik, Physics of Meteor Flight in the Atmosphere (Interscience Publishers, New York, 1958.)

4. F. Verniani and G. S. Hawkins, Astrophys. J. 140, 1590 (1964).

5. J. F. Friichtenicht, Rev. Sci. Instr. 33, 209 (1962).

6. J. C. Slattery, J. F. Friichtenicht, and B. Hamermesy, AIAA Journ. 2, 543 (1964).

7. D. O. Hansen and N. L. Roy, Nucl. Instr. and Methods, 40, (1966), pp 209-212.

8. F. Verniani, Smithsonian Ap. Obs., Special Report No. 145 (1964).

9. D. M. Lazarus and G. S. Hawkins, Smithsonian Constr. Ap. 7, 221 (1963).

NASA-Langley, 1967 —— 24 CR-775